Biosensors and Bioelectronics 133 (2019) 177–182

Contents lists available at ScienceDirect

Biosensors and Bioelectronics

journal homepage: www.elsevier.com/locate/bios

An aptamer-based hook-effect-recognizable three-line lateral flow biosensor for rapid detection of thrombin

Ya Gao[a,b], Ziyu Zhu[a,b], Xiaoxue Xi[a,b], Tingwei Cao[a,b], Wei Wen[a,b], Xiuhua Zhang[a,b], Shengfu Wang[a,b,*]

[a] Hubei Collaborative Innovation Center for Advanced Organic Chemical Materials, Hubei University, Wuhan 430062, China
[b] Ministry-of-Education Key Laboratory for the Synthesis and Application of Organic Functional Molecules, College of Chemistry and Chemical Engineering, Hubei University, Wuhan 430062, China

ARTICLE INFO

Keywords:
Point-of-care
Lateral flow biosensor
Hook-effect
Diagnostic test
Aptamer

ABSTRACT

In this paper, a three-line LFB was successfully developed by adding a thrombin line to a conventional two-line LFB for the detection of thrombin in a wide range of human serum. We introduced a thrombin line between the test line and the control line. The concentration of thrombin in the sample was quantitatively related to the signal formation on the three lines of the LFB. We can make use of signal on three lines to quantitative determinate the thrombin by data processing. The detection range of thrombin concentrations measured in 10 min was 1 nM to 100 μM and the LOD was 0.85 nM. Our approach paves way for rapid and sensitive thrombin detection and a superior device for testing in a wide range of physiological concentrations, which also can be used in other hook-effect-limited aptamers or antibodies based sandwich LFBs, and has a high accuracy even within the range of the hook-effect.

1. Introduction

Lateral flow biosensors (LFBs) for point-of-care (POC) diagnostics are receiving increasing attention due to their features of being cost-effective, time-saving, easy-to-operate, and portable. Since the progress of the first human chorionic gonadotrophin (HCG) immunoassay on LFB platform in 1985 (Jones and Kraft, 2004), LFBs aimed at varied analytes have been successfully developed in the past few years (Posthuma-Trumpie et al., 2009; Wang et al., 2016). Most of these LFBs are based on immunoassays (Hwang et al., 2016). Subsequently, aptamer-based LFBs emerged as an alternative to antibodies-based LFBs (Wu et al., 2018a, 2018b; Jin et al., 2018; Zhao et al., 2018). Aptamers are short single-stranded DNA or RNA in length from 10 to 100 bases which are capable of recognizing various targets via adaptive changes of conformation. As a kind of molecular recognition element, aptamers have been selected to identify various targets which covered metal ions, viruses, large molecules, proteins, and small organic compounds, etc (Ellington and Szostak, 1990; Sullenger and Gilboa, 2002; Fischer et al., 2007; Gao et al., 2014). Researchers have realized aptamer-based detection by adopting strategies such as electrochemical method (Lai et al., 2007; Swensen et al., 2009; Bagheri et al., 2015; Hashemi et al., 2017), fluorescent (Deng et al., 2018; Zhang et al., 2018; Wu et al., 2017), surface-enhanced Raman scattering (Gao et al., 2017a, 2017b; Fu et al., 2016), colorimetric (Chen et al., 2014a, 2014b; Ho and Leclerc, 2004), and electrochemiluminescence (ECL) (Khoshfetrat et al., 2018). The similar recognition characteristics of aptamers and antibodies caused their analogously application in biosensors (Chen and Yang, 2015; Chen et al., 2014). But it is believed that nucleic acid aptamers are promising alternatives to antibodies, which have been widely used in point-of-care diagnostic tests due to their high stability, easy-to-modify and flexibility compared with antibodies (Famulok et al., 2000; Cho et al., 2008; Cass and Zhang, 2011; Dalirirad and Steckl, 2019). The sandwich-type assay is the most frequently used formats in both antibodies-based and aptamers-based LFBs. These methods provide reliable tests for various kinds of targets, but the detection range is often limited by the so-called hook effect. The hook effect refers to the phenomenon of false negative due to the inappropriate proportion of antigen and antibody, wherein the excess of antibody is called the prozone effect; the excess of antigen is called the posterior band effect (Greenberg and Jeejeebhoy, 1989). The contributing factor of high-dose hook effect in LFBs is that the excessive unlabeled analytes occupied the reaction sites on the test line in advance. With the increasing of analytes concentration, the test line signal not rise higher or even reduces. Therefore, the aptamers-based LFBs

* Corresponding author at: Hubei Collaborative Innovation Center for Advanced Organic Chemical Materials, Hubei University, Wuhan 430062, China.
E-mail address: wangsf@hubu.edu.cn (S. Wang).

https://doi.org/10.1016/j.bios.2019.03.036
Received 27 January 2019; Received in revised form 10 March 2019; Accepted 18 March 2019
Available online 19 March 2019
0956-5663/

cannot quantify analytes in a relatively high concentration range, producing inaccurately low results or even false-negative. There are varieties of biological markers which have broad physiological concentration ranges in vivo, are influenced by the high-dose hook effect in clinical test (Namburi et al., 2014; Gillet et al., 2009; Tate and Ward, 2004; Rodbard et al., 1978). Serial sample dilution is most commonly used under the circumstances. Nevertheless this method is time-consuming and cannot distinguish the difference of the outputs between low concentration and over-high concentration essentially. To address the problem, we developed a sandwich type of aptamer-based LFBs which is capable of eliminating the limitation of the hook effect and broadening the detection range. In this paper, thrombin was selected as an analyte to demonstrate our design. Protein molecules detection has gradually become more and more concerned in scientific research and clinical diagnosis. As a kind of serine protease, thrombin plays a pivotal role in blood coagulation and thrombosis. The thrombin binding aptamer is screened in vitro, it can be combined with thrombin in a stable and selective manner. Abnormal concentration of thrombin in blood is associated with blood disease.

Herein, we introduce a versatile method to detect analytes in a wide range of concentrations by assembling a new aptamer-based three-line LFBs. The sensing mechanism is based on a target line added between control line and test line to conventional LFBs.

2. Experimental section

2.1. Materials and apparatus

$HAuCl_4{\cdot}3H_2O$, $Na_3C_6H_5O_7{\cdot}2H_2O$, sucrose, Tween-20, trehalose, deoxyadenosine triphosphate (DATP), Tris (2-carboxyethyl) phosphine (TCEP), TritonX-100 were bought from Sigma-Aldrich (USA). Albumin from bovine serum (BSA) was ordered from Aladdin (Shanghai, China). Thrombin (TB) from human plasma, streptavidin (SA) was ordered from Promega (USA). The nitrocellulose membrane (HFC13502, HFB18002, HFC18002) was obtained from Millipore (Billerica, MA). Adhesive backing pad and absorbent pad (Polyester fiber membrane VL78, CH27), CTD300P automatic strip cutting machine, DT2032 strip analyzer and HM3030 dispenser were from KinbioTech. Co., Ltd. Shanghai. The 20 × phosphate buffer saline (pH 7.4–7.6, nuclease-free) and sodium chloride-sodium citrate buffer (20 × SSC, pH 7) used in the experiment were purchased from Sangon (Shanghai, China) company. The desktop high-speed refrigerated centrifuge (Sigma3–18KS) is purchased from Sigma Co., Ltd. German. The nanoparticles were characterized with a transmission electron microscope (TEM, FEI Tecnai G20, USA) at an acceleration voltage of 200 kV. The single-stranded DNAs and modified DNAs sequences are shown in Table S2.

2.2. Preparation of Au NPs

Gold nanoparticles (Au NPs) with an average diameter of 15 ± 2.5 nm were synthesized and applied in whole work, for reason that Au NPs with this diameter range has superior performance on LFAs according to the literature described previously (Qin et al., 2015a, 2015b). The preparation procedure of Au NPs was referred to the conventional reduction method (Xu et al., 2008). Glassware were soaking with new prepared aqua regia (V_{HCl} /V_{HNO3} = 3/1) for 30 min and washed thoroughly in advance, then rinsing with ultra-pure water (DI, > 18.25 MΩ cm) for several times until the glassware was no aqua regia residue and oven-dried. 100 mL $HAuCl_4$ solution with a mass fraction of 0.01% was heated to bumping with stirring. Next, 2.7 mL trisodium citrate solution (1 wt%) was quickly added into the solution. The solution became wine red in a few minutes, turned off the heat and continued stirring for an additional 15 min. Finally, the nanoscale gold particles with an average diameter of 15 ± 2.5 nm were obtained.

The TEM photo of gold nanoparticles came from the FEI Tecnai G20 transmission electron microscope (USA). As shown in the Fig. 2, the average diameter was 15 ± 2.5 nm, and the particle size and shape were relatively uniform. The optical properties of Au NPs are attributed to the collective oscillation of the surface conduction electrons in response to optical excitation, which is called localized surface plasmon resonance (LSPR). The surface-plasmon band in the visible region of the spectrum is responsible for the remarkable colors of Au NPs colloidal solutions (Alvarez et al., 1997). The resulting colloid of Au NPs has an absorption maximum at ~520 nm (Fig. S1.).

2.3. Preparation of Au-Apt1 conjugates

DNA probe was centrifuged for 2 min at 12000 rpm, and then dissolved to 10 μM with PBS buffer. 80 μL of aptamer probe (Apt1, 10 μM) solution and 40 μL of TCEP (1 mM) were added to 1.2 mL five times concentrated Au NPs colloid (~1.4 mM), stirring for 1 h at room temperature. Subsequently, 80 μL of 15 μM DATP was added continued stirring for 30 min. After the reaction finished, the conjugates were placed under the condition of 4 °C for 4 h and then became stable. TCEP is a highly efficient thiol reductant, which was used to selectively reduce the disulfate linkage between thiol and sulfhydryl groups in this experiment. DATP is a monomer unit of nucleic acid, commonly used as sealant between gold nanoparticles and DNA complexes. The product was centrifuged for 15 min at 12000 rpm, after discarding the supernatant, the conjugates redispersed in 5% PBSB (5 g BSA dissolved in 10 mL PBS buffer). After three times of cleaning with 5% PBSB (the supernatant was discarded), Au-Apt1 conjugates were dispersed in 1.2 mL of buffer consisting of 20 mM $Na_3PO_4{\cdot}12H_2O$, 5% BSA, 0.25% Tween-20, and 10% sucrose, then preserved at 4 °C.

2.4. Fabrication of the lateral flow biosensor

As shown in Fig. 1, the LFB was fabricated by four segments including sample pad, nitrocellulose membrane, absorbent pad, and backing card. Each layer overlaps about 2 mm when fabricating. For sake of smooth flowing of sample solution on paper strip, the sample pad was soaked with the sample buffer (pH = 8.0, 0.25% TritonX-100, 0.02 M Tris-HCl, and 0.15 M NaCl) for one hour to air-dry at room temperature before being assembled. According to the reported method, streptavidin was applied as fixing agent for immobilization of T-DNA and C-DNA onto the NC membrane (Qin et al., 2016; Xu et al., 2008). In particular, T-DNA solution (10 μM) and streptavidin (2 mg/mL) were mixed (volume ratio of 10:1) and cultured at room temperature for 1 h. After the reaction finished, the ultrafiltration centrifuge tubes (30 kD, Millipore's Amicon Ultra-15) were used to remove the excessive T-DNA by abandoning filtrate in the outer tube. The average pore size of ultrafiltration membrane (UF membrane) is larger than DNA probe, but smaller than streptavidin, so that excess DNA was separated from complex solution during centrifugation. Subsequently, the C-DNA was treated in accordance with T-DNA. The two solutions were sprayed to the NC membrane by HM3030 scribing instrument to form the T line and the C line. The median line between T line and C line was drawn on a target line with thrombin solution (1 mg/mL), and the distance between two adjacent lines was 5 mm. A control line was printed to validate assay function for the detection of thrombin. Then the membrane was natural drying and stored at 4 °C. Finally, three layers of membrane were pasted on a common backing card by overlapping 2 mm. After the assembly was completed, the CTD300P automatic strip cutter was used to cut the paper strips into 4 mm wide and stored under the condition of 4 °C.

2.5. Detection process on lateral flow biosensor

Sample solution containing desired concentrations of thrombin were prepared with running buffer (4 × SSC, 5% BSA) according to the literature (Xu et al., 2008). The Au-Apt1 conjugates and thrombin sample solution were mixed and cultured for 2 h. A 10 μL portion of

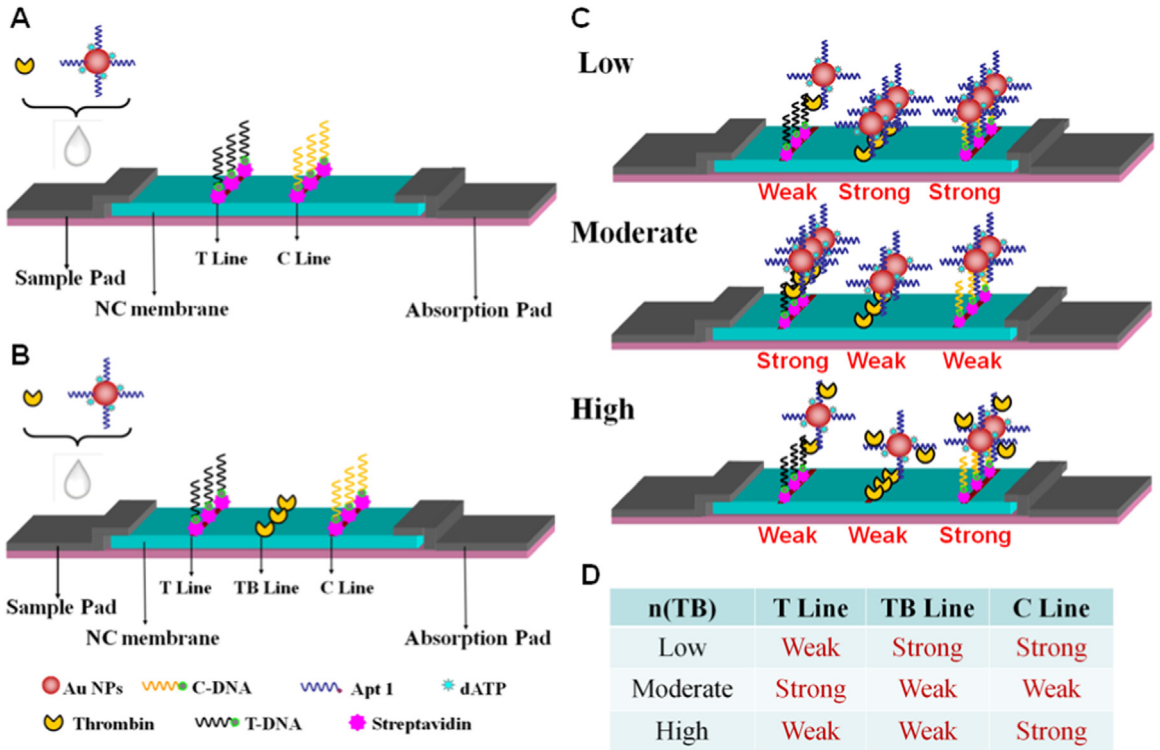

D

n(TB)	T Line	TB Line	C Line
Low	Weak	Strong	Strong
Moderate	Strong	Weak	Weak
High	Weak	Weak	Strong

Fig. 1. Schematic representation of configuration of the test biosensors. (A) Traditional two-line nucleic acid lateral flow biosensors. (B) New type of three-line nucleic acid lateral flow biosensor. "TB line" stands for thrombin line. (C) Interpretation of results under low, moderate and high concentration of thrombin (TB). (D) Correspondence table between the level of TB concentration in the analyte and the intensity of the three lines on the biosensor.

mixture was dropwise added onto the sample pad, 10 μL of running buffer (4 × SSC, 5% BSA) was added after 2 min, and an additional wash was performed after another 2 min. Finally distinct red bands appeared in 15 min. Then with the Kinbio analysis software installed on the computer, the images on the LFB were processed and analyzed. The output peak area was applied to quantify the target.

3. Results and discussion

3.1. Design principle of lateral flow biosensor

In this work, we developed a lateral flow biosensor for the detection of thrombin in a wide detection range. A test line, a target (thrombin) line and a control line were deposited onto the NC membrane respectively (Fig. 1B). And specifically, the target line played a significant role in this system, for reason that it can assist in discrimination between high-dose and low-dose of analyte when the hook effect emerged.

To be specific, as shown in Fig. 1C, when the mixture was dripped to the sample pad, the solution wet the sample pad and moved to the absorption pad driven by the capillary action. In the presence of low concentration of thrombin, the mixture of sample and Au-Apt1 migrated through the test line, a small quantity of thrombin conjugated with Au-Apt1 were captured on T-DNA aptamer and generated a weak red band on T line. When the mixture migrated through target line, the mixture still contained abundant residual Au-Apt1, which would be captured by thrombin on target line and formed a strong red band. As the liquid continued to migrate, spare Au-Apt1 became comparative less, Au-Apt1 were captured by C-DNA and via the principle of Watson-Crick base pairing, forming a red band slight weaker than TB line, but much stronger than T line.

In the present of moderate concentration of thrombin in the sample, when the mixture flowed past the test line, relatively more conjugation would be captured by T-DNA on thrombin aptamer and generated strong red band on the T line. When the mixture continuously migrated through the target line, the residual unreacted Au-Apt1 conjugates were captured by the thrombin line, forming a weak red band. As the liquid flowed to the C line, an even smaller amount of remnant Au-Apt1 conjugates were captured by C-DNA and a weaker red band was formed on the control line.

In the presence of ultrahigh concentration of thrombin, there would be a large number of unreacted thrombin in the mixture after the combination of Au-Apt1 conjugates and thrombin. In the process of sample application, the migration rate of unreacted TB was faster on the NC membrane due to their smaller size compared with TB conjugated with Au-Apt1. Therefore, unreacted TB molecule occupied the reactive site on T-DNA in advance, and the sandwich detection of TB was inhibited, which resulted in a weak red band on the T line. When the mixture continued to migrate through the target line, most of Au-Apt1 conjugates were bonded to excess TB from sample solution. So it inhibited the reaction with TB on the target line, which resulted in weak red band. Au-Apt1 conjugates and thrombin were captured on T line owing to the recognition reactions between the aptamer (fragment: GGT TGG TGT GGT TGG) and thrombin. But Au-Apt1 were captured by C-DNA and via the principle of Watson-Crick base pairing. Consequently, the response on the control line is unaffected. A large amount of Au-Apt1 conjugates was captured by C-DNA and a stronger red band formed on the control line.

As shown in Fig. 1D, when the target is low-dose and overdose, the signal intensity of T line and C line clearly resemble. So the accurate target concentration cannot be identified simply rely on the signal of T line and C line. The same signal intensity on the T line can correspond to the lower and higher two target concentrations, even the false negative. To distinguish the high-dose hook effect, we added a thrombin line (TB line) between traditional test line and control line. First, the test line signal was quantitative analyzed by corresponding equation. And two results were received. Finally, we determined the interval of target concentration based on the signal intensity of the target line, which determines the choice between the low-dose and high-dose

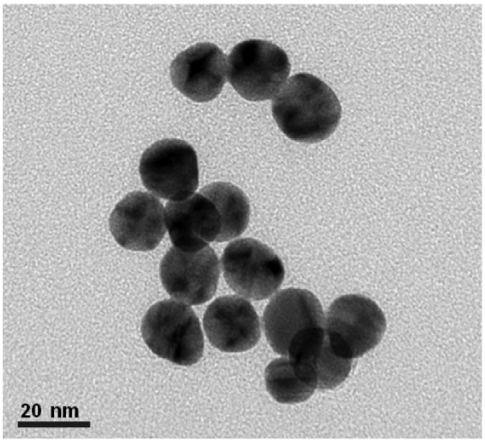

Fig. 2. TEM image of Au NPs.

results. In the principle mentioned above, we broadened the detection range of target in a simple manner. (Fig. 2).

3.2. Optimization of experimental conditions

Assay optimization included dosage of Apt1 used to modify Au NPs (Fig. 3A), effect of spacer in Apt1 (Fig. 3B), selection of nitrocellulose membrane type (Fig. 3C), optimal concentration of BSA buffer (Fig. 3D). The signal was observed in the presence of 20 nM thrombin.

In this experiment, Au NPs were used as the colorimetric label, Apt1 was modified with sulfhydryl group for binding to Au NPs, thiolate DNA fixed on the surface of Au NPs via self-assembly process by forming Au-S bonds. Naturally, the dosage of Apt1 directly affects the stability of the Au-Apt1 conjugation and the capture efficiency on paper strip. When the DNA coating on Au NPs is incomplete, it is unstable in the washing process which causes aggregation and sedimentation easily. In addition, insufficient modification of Au NPs leads to low capture efficiency of target, ultimately affects the sensitivity of the lateral flow biosensor. Therefore, we added different volumes of Apt1 solution (10 μM) to 1200 μL five-times concentrated Au NPs and observed the magnitude of intensity of the assay readout. The peak area and the signal to noise ratio (P/N) were applied as the two major criteria for measuring the performance of the test in Fig. 3.

While the volume of Apt1 solution increases from 20 μL to 80 μL, the signal increases and reaches the platform at 80 μL. Subsequently, with the continuous increase of Apt1 addition, significant signal attenuation was found, which is due to the interfusion of the PBS buffer in the compounding process with Apt1 solution. Large dosage of Apt1 solution introduced plenty of sodium ions simultaneously. The gold nanoparticles produced aggregation effect, which caused a great impact on the synthesis process. In addition, the variation trend of P/ N ratio is in accordance with peak area. Finally, we chose 80 μL Apt1 solution to react with 1200 μL five times concentrated gold nanoparticles.

In order to capture target and form red band on T line, three kinds of probes (thrombin aptamer Apt1, T-DNA and C-DNA) were designed in this work. The base sequence of three probes will also affect sensitivity because of steric hindrance in the process of identifying and capturing. Theoretically, a spacer chain (the continuous A base is used in this experiment) will alleviate the steric hindrance when combined with thrombin molecules. To validate and optimize this, we performed experiments using different sequences of Apt1 and T-DNA, and examined and compared the results. Results shows that spacer chains was needed in capture probes.

The most important element in lateral flow biosensor is the

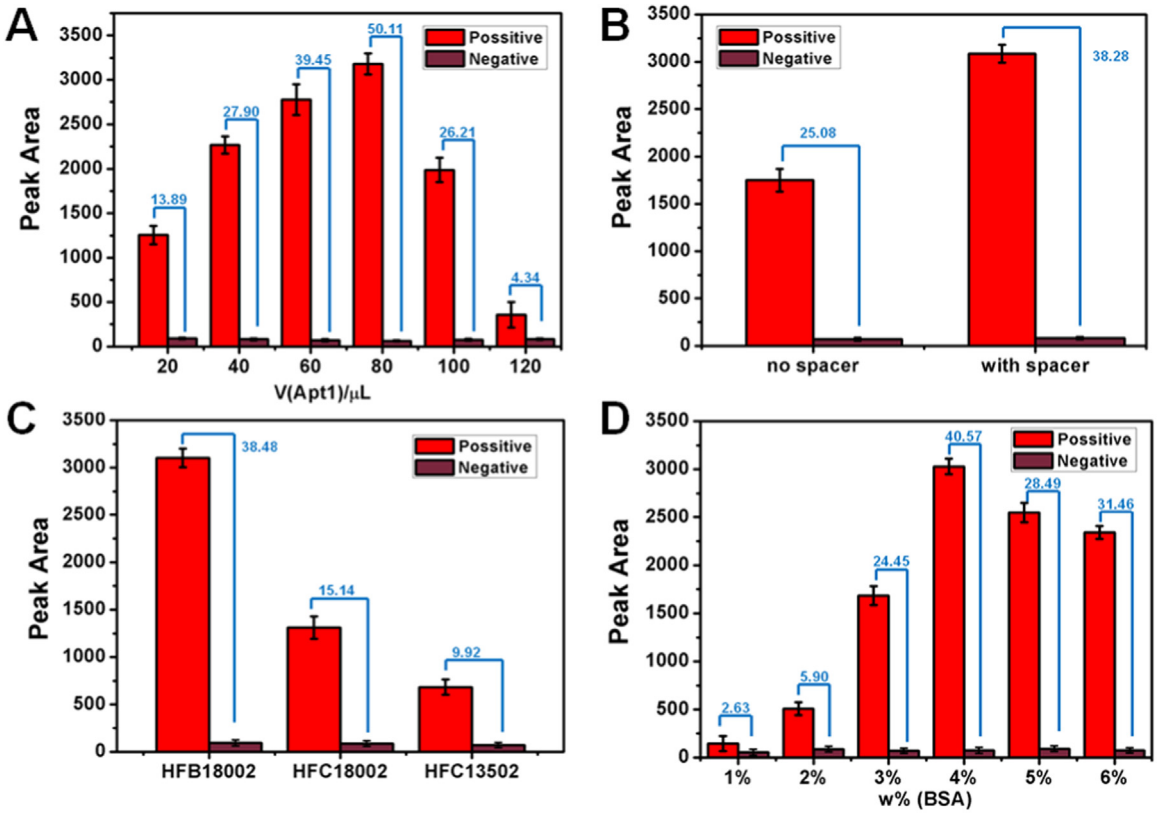

Fig. 3. Optimization of the assay conditions (A)Effect of dosage of Apt1 used to modify AuNPs on the signal of lateral flow biosensors. (B) The effect of spacer in Apt1 on the signal of lateral flow biosensors. (C) Effect of the type of nitrocellulose membrane on the signal of lateral flow biosensors. (D) Effect of the ratio of BSA in buffer. Figure in blue represents P/N ratio (positive to negative signal). Error bars indicate the standard errors of three independent experiments. (For interpretation of the references to color in this figure legend, the reader is referred to the web version of this article).

nitrocellulose membrane. Since different NC membrane types have different pore sizes, the flow rates are also different, which affects the reaction efficiency and leads to differences in sensitivity. To achieve high signal strength and P/N ratio (the ratio of positive to negative signal), we applied three commercially available nitrocellulose membranes (Mill-ipore HFB18002, HFC18002 and HFC13502) to the three-line LFB. As shown in Fig. 3C and Table S1, the LFB using the HFB18002 nitrocellulose membrane performed best, so it was chosen for this work.

During the synthesis of the Au-Apt1 conjugates, excess Apt1 probe may exist in the mixture. If the composite is used for sample application without cleaning, excess Apt1 will migrate faster on the LFB than the Au-Apt1 conjugates due to its smaller weight and volume, and react with probes on the T and C lines in advance. The situation makes it difficult for Au-Apt1 conjugates and the target thrombin to be captured on T and C lines. Therefore, after the composite was synthesized and stabilized, it was centrifuged and the supernatant was replaced with the cleaning solution for several times to remove unreacted Apt1. In this experiment, we selected PBSB (PBS buffer + BSA) as a complex cleaning solution and optimized the BSA content. Specifically, we tried PBSB cleaning solutions with different mass fractions (w% = 1, 2, 3, 4, 5, 6). As shown in Fig. 3D, by comparing the peak area and P/N ratio of T-line in the presence of the 20 nM thrombin, we finally selected PBSB cleaning solution containing 4% BSA. (Fig. 4).

3.3. Detection performance of lateral flow biosensor

By measuring different concentrations of thrombin samples, we found that the peak area on the T line and the logarithm of the thrombin concentration was closely matched to the quadratic equation between 1 nM and 500 nM and exhibited a good correlation coefficient ($R^2 = 0.9527$). The experiment performed three repeated measurements at each target concentrations to obtain error bars. In the actual quantification, two different concentration results were generated by the quadratic formula from the calibration curve. We first compared the intensity of the target (TB) line and the control line. If the response of target line is stronger, we selected the lower value, whereas we selected the higher value in the converse case. The relationship curve is quantified. In this way, our work widens the detection range from 1 nM to 100 μM with a detection limit of 0.85 nM (LOD, blank signal + 3 standard deviations). By contrast, the responses range of a conventional two-line LFB was 5–100 nM of thrombin with a detection limit of 2.5 nM according to literature (Xu et al., 2008).

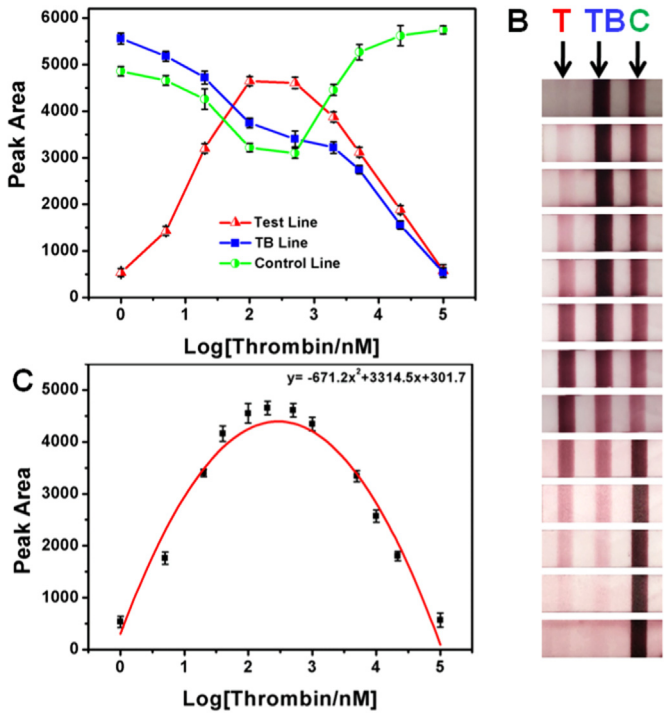

Fig. 4. (A) Signal response trend graph of three lines on lateral flow biosensors against different concentrations of TB; (B) Photograph of TB detection in PBS; (C) Response for TB detection. Error bars indicate the standard errors of three independent experiments.

3.4. Repeatability and stability analysis

The accuracy and reproducibility of the proposed method were evaluated by performing intra-assay and inter-assay reproducibility studies (Table S3). We analyzed three standard samples with low (10 nM), medium (500 nM) and high (10 μM) levels of TB concentrations. Intra-assay analysis was performed within one day, with five samples per concentration. At the same time, the measurement was performed every two days and repeated five times. According to Table S3, the CV values measured within the group and between the groups were 4.77–6.94 and 4.05–6.33, respectively, indicating good accuracy and reproducibility. Therefore, this method has a good potential for further application.

In order to observe the stability of the LFB, we tested the strips of different storage time. It can be seen from the signal on the T line that the signal intensity of the preserved LFB was close to slightly weakened (Fig. 5), indicating that the LFB performed good analytical stability.

3.5. Analysis and application of lateral flow biosensor

In order to further prove the reliability and practicability of the proposed three-line LFB, we carried out the spike recovery experiment. Different concentrations of TB were spiked into the blank human plasma samples and then measured by the LFB. As shown in Table S4, with the increase of TB concentration, the average recoveries of analytes were between 92.00% and 108.92%, which indicated that the LFB has good accuracy.

4. Conclusion

In this experiment, we constructed a hook-effect-recognizable three-line lateral flow biosensor. The assay was designed to detect the thrombin in a relatively wide range by introducing a target line to conventional two-line LFB. All the other conditions are basically the same as those used in conventional LFB. The thrombin level in the test sample is generated by the data processing from the itensity of the three lines. Under optimal conditions, a detection range of the concentration of thrombin in 10 min was 1 nM to 100 μM, and the detection limit

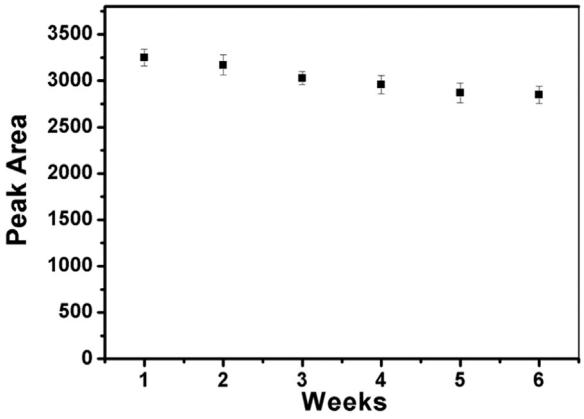

Fig. 5. Stability test of the three-line lateral flow biosensor. Error bars indicate the standard errors of three independent experiments.

(LOD) was 0.85 nM. Compared with the analytical performances of traditional two-line LFBs, the proposed three line LFBs is capable of eliminating the influence of hook effect, widening the discernible detection range. The platform enabled rapid, low-cost and portable testing, even holds great potential as a field tool for detection in a wide range of physiological concentration and can be a versatile method for other analytes in future research.

CRediT authorship contribution statement

Ya Gao: Funding acquisition, Formal analysis, Writing - original draft. **Ziyu Zhu:** Funding acquisition, Formal analysis, Writing - original draft. **Xiaoxue Xi:** Funding acquisition, Formal analysis, Writing - original draft. **Tingwei Cao:** Funding acquisition, Formal analysis, Writing - original draft. **Wei Wen:** Writing - review & editing. **Xiuhua Zhang:** Writing - review & editing. **Shengfu Wang:** Writing - review & editing.

Acknowledgements

This work was supported by the National Natural Science Foundation of China (No. 21475032).

Declaration of interests

None.

Appendix A. Supporting information

Supplementary data associated with this article can be found in the online version at doi:10.1016/j.bios.2019.03.036.

References

Alvarez, M.M., Khoury, J.T., Schaaff, T.G., Shafigullin, M.N., Vezmar, I., Whetten, R.L., 1997. J. Phys. Chem. B 101 (19), 3706–3712.
Bagheri, H., Talemi, R.P., Afkhami, A., 2015. RSC Adv. 5 (72), 58491–58498.
Cass, A.E., Zhang, Y., 2011. Faraday Discuss. 149 (1), 49–61.
Chen, A., Yang, S., 2015. Biosens. Bioelectron. 71, 230–242.
Chen, Z., Tan, Y., Zhang, C., Yin, L., Ma, H., Ye, N., Hong, Q., Lin, Y., 2014. Biosens. Bioelectron. 56, 46–50.
Chen, J., Zhou, S., Wen, J., 2014. Anal. Chem. 86 (6), 3108–3114.
Cho, H., Baker, B.R., Wachsmann-Hogiu, S., Pagba, C.V., Laurence, T.A., Lane, S.M., Lee, L.P., Tok, J.B.H., 2008. Nano Lett. 8 (12), 4386–4390.
Dalirirad, S., Steckl, A.J., 2019. Sens. Actuators B-Chem. 283, 79–86.
Deng, X., Wang, C., Gao, Y., Li, J., Wen, W., Zhang, X., Wang, S., 2018. Biosens. Bioelectron. 105, 211–217.
Ellington, A.D., Szostak, J.W., 1990. Nature 346, 818–822.
Famulok, M., Mayer, G., Blind, M., 2000. Acc. Chem. Res. 33 (9), 591–599.
Fischer, N.O., Tarasow, T.M., Tok, J.B.H., 2007. Curr. Opin. Chem. Biol. 11, 316–328.
Fu, X., Cheng, Z., Yu, J., Choo, P., Chen, L., Choo, J., 2016. Biosens. Bioelectron. 78, 530–537.
Gao, X., Zheng, P., Kasani, S., Wu, S., Yang, F., Lewis, S., Nayeem, S., Engler-Chiurazzi, E.B., Wigginton, J.G., Simpkins, J.W., Wu, N., 2017a. Anal. Chem. 89 (18), 10104–10110.
Gao, Y., Deng, X., Wen, W., Zhang, X., Wang, S., 2017b. Biosens. Bioelectron. 92, 529–535.
Gao, X., Xu, H., Baloda, M., Gurung, A.S., Xu, L.P., Wang, T., Zhang, X., Liu, G., 2014. Biosens. Bioelectron. 54, 578–584.
Gillet, P., Mori, M., Van Esbroeck, M., Van den Ende, J., Jacobs, J., 2009. Malar. J. 8 (1), 271.
Greenberg, G.R., Jeejeebhoy, K.N., 1989. Reply. Gut 30 (3), 422–423.
Hashemi, P., Bagheri, H., Afkhami, A., Ardakani, Y.H., Madrakian, T., 2017. Anal. Chim. Acta 996, 10–19.
Ho, H.A., Leclerc, M., 2004. J. Am. Chem. Soc. 126 (5), 1384–1387.
Hwang, J., Lee, S., Choo, J., 2016. Nanoscale 8 (22), 11418–11425.
Jin, B., Yang, Y., He, R., Park, Y.I., Lee, A., Bai, D., Li, F., Lu, T.J., Xu, F., Lin, M., 2018. Sens. Actuators B-Chem. 276, 48–56.
Jones, G., Kraft, A., 2004. Bus. Hist. 46 (1), 100–122.
Khoshfetrat, S.M., Bagheri, H., Mehrgardi, M.A., 2018. Biosens. Bioelectron. 100, 382–388.
Lai, R.Y., Plaxco, K.W., Heeger, A.J., 2007. Anal. Chem. 79 (1), 229–233.
Namburi, R.P., Kancherla, V., Ponnala, A.R., 2014. J. NTR Univ. Health Sci. 3 (1), 5.
Posthuma-Trumpie, G.A., Korf, J., van Amerongen, A., 2009. Anal. Bioanal. Chem. 393 (2), 569–582.
Qin, C., Gao, Y., Wen, W., Zhang, X., Wang, S., 2016. Biosens. Bioelectron. 79, 522–530.
Qin, C., Wen, W., Zhang, X., Gu, H., Wang, S., 2015a. Chem. Commun. 51 (39), 8273–8275.
Qin, C., Wen, W., Zhang, X., Gu, H., Wang, S., 2015b. Analyst 140 (22), 7710–7717.
Rodbard, D., Feldman, Y., Jaffe, M.L., Miles, L.E.M., 1978. Immunochem 15 (2), 77–82.
Swensen, J.S., Xiao, Y., Ferguson, B.S., Lubin, A.A., Lai, R.Y., Heeger, A.J., Plaxco, K.W., Soh, H.T., 2009. J. Am. Chem. Soc. 131 (12), 4262–4266.
Sullenger, B.A., Gilboa, E., 2002. Nat. Rev. 418, 252–258.
Tate, J., Ward, G., 2004. Clin. Biochem. Rev. 25 (2), 105.
Wang, X., Choi, N., Cheng, Z., Ko, J., Chen, L., Choo, J., 2016. Anal. Chem. 89 (2), 1163–1169.
Wu, Z., He, D., Xu, E., Jiao, A., Chughtai, M.F.J., Jin, Z., 2018a. Food Chem. 269, 375–379.
Wu, S., Liu, L., Duan, N., Li, Q., Zhou, Y., Wang, Z., 2018b. J. Agric. Food Chem. 66 (8), 1949–1954.
Wu, Z., Shen, H., Hu, J., Fu, Q., Yao, C., Yu, S., Xiao, W., Tang, Y., 2017. Anal. Bioanal. Chem. 409 (22), 5209–5216.
Xu, H., Mao, X., Zeng, Q., Wang, S., Kawde, A.N., Liu, G., 2008. Anal. Chem. 81 (2), 669–675.
Zhang, J., Lv, X., Feng, W., Li, X., Li, K., Deng, Y., 2018. Microchim. Acta 185 (8), 364.
Zhao, S., Wang, S., Zhang, S., Liu, J., Dong, Y., 2018. Chin. Chem. Lett. 29 (11), 1567–1577.